INTERNATIONAL JOURNAL OF NOVEL RESEARCH AND DEVELOPMENT (IJNRD)
© 2026 IJNRD | Volume 11, Issue 3, March 2026 | ISSN: 2456-4184 | IJNRD.ORG

Wireless Power Transmission System of Video Capsule Endoscopy

Dr. Pramila Mishra ***(kdmishra2004@gmail.com)***

Department of Applied Science & Engineering, Barkhatullah University, Bhopal, India

Abstract- Wireless Capsule Endoscopy (WCE) provides a means to obtain a detailed video of the small intestine. A single session with WCE may produce nearly 8 hours of video. Its interpretation is tedious task, which requires considerable expertise and is very stressful. The Model of Deformable Rings (MDR) was developed to pre-process WCE video and aid clinicians with its interpretation. The MDR uses a simplified model of a capsule's motion to flexibly match (register) consecutive video frames. Essentially, it computes motion descriptive characteristics and produces a two-dimensional representation of the gastrointestinal (GI) tract's internal surface. The motion-descriptive characteristics are used to indicate video fragments which exhibit seminary contractions, peristalsis, refraction phases and areas of capsule retention. The experimental results demonstrate that the number of discovered pathologies and gastrointestinal landmarks increases with the MDR technique.

Keyword- Video Capsule endoscope; inductive coupling; Helmholtz coil

I. INTRODUCTION

The first wireless capsule endoscope was launched in 2001 by Given Imaging Ltd, and reported in an article in "Nature" (Iddan et al., 2000) [1]. Since the device received FDA (American Food & Drug Administration) clearance in August 2001 [2, 3] over 400000 examinations globally have been conducted. The 11mm x 26mm M2A capsule is propelled passively, hence having been swallowed, it is propelled through the food tract by normal peristaltic movement of the human gastrointestinal (GI) [4,5] system, usually reaching the colon, before being expelled naturally from the body. One end of the capsule contains an optical dome with six white Light Emitting Diodes (LEDs) and a CMOS camera that captures 2 images (circular shape from a square of 256 × 256 pixels) a second. These images are compressed using JPEG and relayed via a transmitter using radio frequency signal (approximately 432 MHz) to an array of aerials, which are attached to the patient's body, from where they are transferred over the wires to a data-recorder. The sensor array allows for continues triangulation of the position of the capsule inside the body of the patient so that the trajectory of the capsule passage can be later displayed on the workstation monitor. The accuracy of the capsule location provided by this method was reported to be ±3 cm (Ravens and Swain, 2002) [6-9].

II. WCE Clinical Importance

The gastrointestinal (GI) tract shown in Figure consists of the oesophagus, stomach and duodenum (upper GI tract), the jejunum, ileum (small bowel), colon and rectum. In this section we describe the different feature extraction methods which were employed for the WCE video segmentation task. These methods utilise Colour, Texture and Motion information contained in the capsule exams and are describe in detail. The distribution of colours in an image provides a useful cue for image indexing and object recognition. The colour distribution histogram is the most commonly used method of representing image colour information. A short inspection of capsule images suggests that texture features can play an important role in the topographic video segmentation. The most prominent texture pattern that distinguishes different organs is the villi - the small finger-like projections, responsible for food absorption, which are present in the small intestine, but not in the neighbouring regions of stomach and colon. Texture patterns in the mouth and oesophagus are also very distinctive. Moreover, there are a number of fluids such as saliva, bile and digestive remains, each possessing a different textural pattern [10].

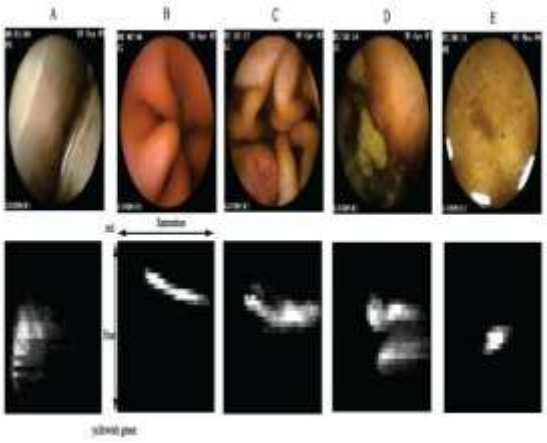

Figure 1: WCE images acquired from A) Mouth B) Stomach, C) Small Intestine, D) Partially occluded Colon E) completely occluded Colon with histogram.

Let us consider a grey-scale image whose intensity can be written I(x, y). The N neighbours of any given pixel p can be denoted as n^i, i = 0..., N − 1. In order to calculate an LBP value, the value of each neighbour n^i is compared to the value of 'p' to establish whether it is greater than or less than 'p'. This can be written as a function mapping each n^i onto a value b_i as follows:

$$b_i = \begin{cases} 1 \ if \ n^i \geq p \\ 0 \ if \ n^i < p \end{cases}$$

The LBP value for pixel (x_0, y_0) is calculated by concatenating the N binary values into a bit number, which can be described as follows:

$$\mathbf{LBP}(x_0, y_0) = \sum_{i=0}^{N-1} b_i 2^i$$

Moreover, following , we calculate LBP, which is invariant

to image rotations and reduces the number of possible patterns:

$$\mathbf{LBPri = min\{ROR(LBP, i)|i = 0, 1, ...,N - 1\}}$$

where the ROR function shifts the N-bit binary LBP value, i bits to the right, with wrap-around. The number of possible patterns can be further reduced by considering only patterns of a specific type. This is achieved by introducing an extra constraint on pattern uniformity. Given the binary string $b_0,b_1...b_{N-1}$, the pattern uniformity is defined as the number of transitions that occur in that string and each transition a change from 0 to 1 or vice-versa including wrap-around.

$$\mathbf{Uniformity} = \|\mathbf{b_o} - \mathbf{b_{N-1}}\| + \sum_{\mathbf{i=0}}^{\mathbf{N-2}} \|\mathbf{b_i} - \mathbf{b_{i+1}}\|$$

A brief observation of any capsule video clearly suggests that the motion patterns differ in different organs. At the entrance, we can distinguish two phases: the first phase takes place when the capsule is outside the body of the patient, in which case we cannot predict much about its motion since the capsule may be waiting to be picked up and swallowed or in the hand of the clinician or the patient in which case, there would be some irregular motion pattern. The second phase begins once the capsule is swallowed by the patient and the capsule travels through the mouth and down the oesophagus with a distinct and quick movement. In the stomach, the capsule first tumbles around, then reaches the bottom of the stomach, where it moves according to the contractions of the pylorus until it traverses the valve and enters the small intestine. There are various cost functions which include Mean Absolute Difference (MAD), Mean Squared Error (MSE) or Peak-Signal-to-Noise-Ratio (PSNR).

$$MAD = \frac{1}{N^2} \sum_{i=1}^{N} \sum_{j=1}^{N} |C_{ij} - P_{ij}|$$

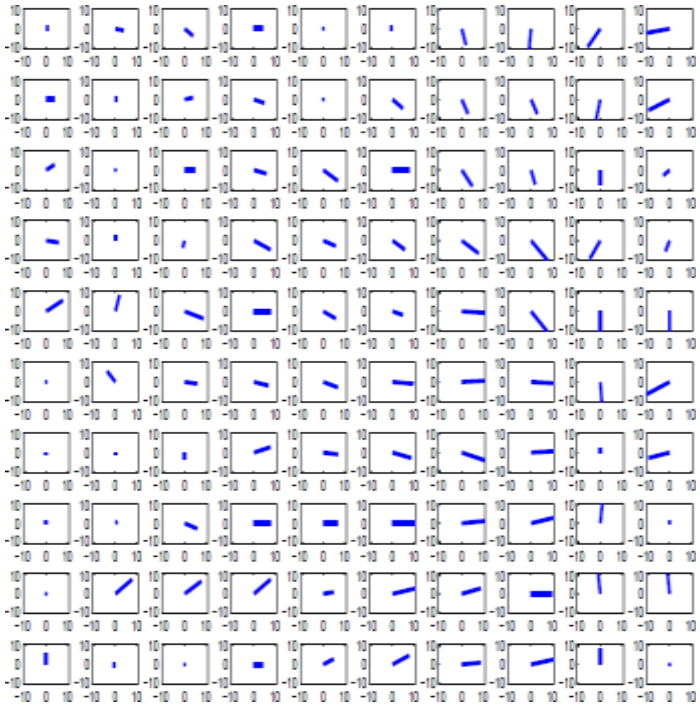

Figure 2: An example of a grid of motion vectors.

It can be seen that most of the vectors point to the right.

1. sum of motion vectors

$$F_1 = \sum_{i=1}^{N} x_i$$

2. sum of vector lengths

$$F_2 = \sum_{i=1}^{N} |x_i|$$

3. sum of the following dot products

$$F_3 = \sum_{i=1}^{N} (x_i u_i)$$

III Principal Component Analysis

The PCA (Pratt, 2001; Gonzalez et al., 2004) [10] of a distribution is also called the (discrete) Karhunen-Loève [11] transform (KLT) or the Hostelling transform. It is the only optimal linear transformation for keeping the subspace that has largest variance. However, computational complexity of PCA (O (M_2N_2)) is higher when compared, for example to the DCT discussed above (O(M_N log $2M_N$)). The basic functions are called the principal components (PCs) which are the convention that will be followed in the rest of this thesis. It is worth noting that unlike other linear transforms (including DCT), PCA does not have a fixed set of basis vectors. It computes the mean vector m_x and forms the covariance matrix, C_x for a distribution x, of size K:

$$\mathbf{M_x} = \frac{1}{k} \sum_{k=1}^{k} x_k$$

Having calculated m_x and C_x, the PCA of a distribution x is given by:

$$\mathbf{Y = A\ (\ x - m_x)}$$

Where the rows of matrix A are the normalised eigenvectors of C_x, ordered according to the decreasing corresponding Eigen values. The covariance matrix of y is a diagonal matrix C_y, whose diagonal elements are the Eigen values of C_x. The inverse transformation (since A is orthonormal, its inverse equals its transpose) produces the reconstructed x:

$$\mathbf{x = A^T y + m_x}$$

With regard to compression, the usefulness of PCA becomes clear when only some subset of q eigenvectors is used, in which case A becomes a q × n matrix Aq. Hence, the approximated reconstruction can be given as follows:

$$\mathbf{X} = A_q^T + \mathbf{m}_x$$

There is an alternative way of calculating PCA which utilises singular value decomposition (Golub and van Loan, 1983) [12] and was used in this work. Here, x denotes the distribution with the subtracted mean, where each column contains a different subject, and each row different variable. Then we can write PCA as:

$$\mathbf{y = u^t x = SV^T}$$

where U,S,V & T is the singular value decomposition of x.

IV. Result

Fig 3 shows a relation between efficiency vs S_0 ,whereS_0 is the enclosed area of each coils. From graph it is clear that efficiency increases exponetiallyas the area of coils increases.But at higher values of S_0 it is almost gets linear it means after this value 6×10-4if enclosed areas increase slightly, you get bigger change in efficiency.

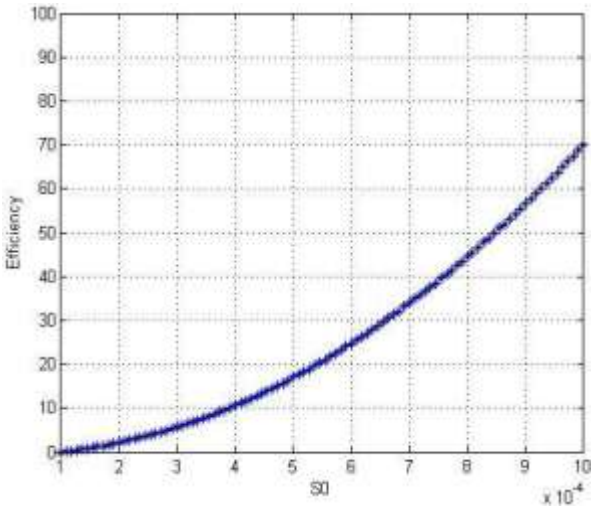

Figure3: S_0 Vs Efficiency.

Fig 4 shows a change between received average power vs S_0, From plot it is clear that as enclosed area increases received power also increases because you get more signals from follower resources as expected mathematically.

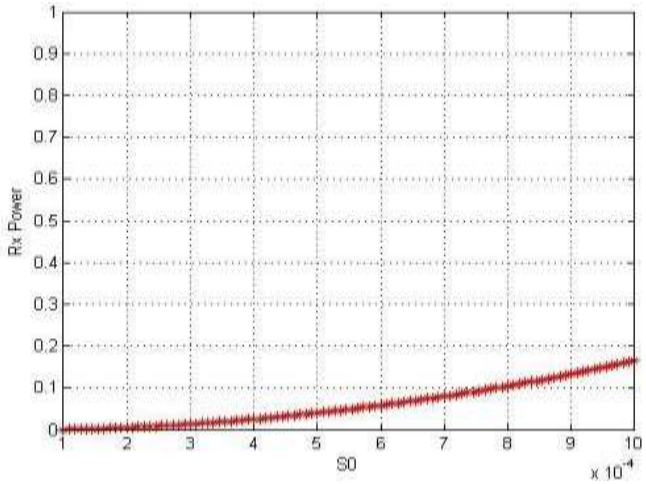

Figure4: S_0 Vs R_x power

The more uniform the magnetic field is, the less the magnetic field uniformity tends to be. The uniformity of different TC structures have been analysed by introducing plot. The result shown in Figure indicates that as the number of turns increases, the magnetic field uniformity of the TC decreases, i.e. the magnetic field becoming more uniform. With the same number of turns, the magnetic field uniformity of Helmholtz coils excels that of the double solenoid pair while the single solenoid pair works worst. In the meantime, the magnetic flux density coefficient of the canter of TC magnetic field leads a linear increase as the number of turns goes up. With the same number of turns, the magnetic flux density coefficient of the single and the double solenoid coils are quite close in numerical value while that of the Helmholtz coils is relatively smaller and the gap wide as the number of turns increases.

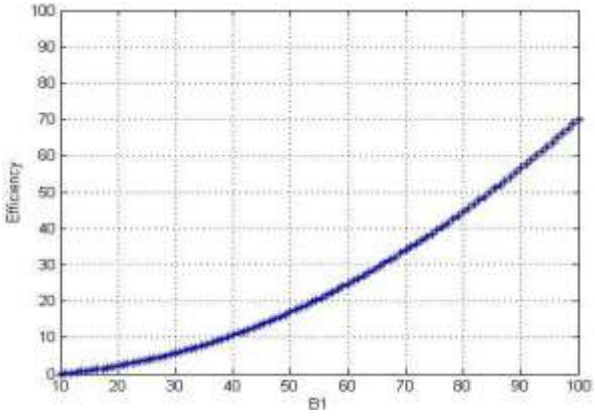

Fig 5 (a) Relation between Efficiency V/s Magnetic field densities

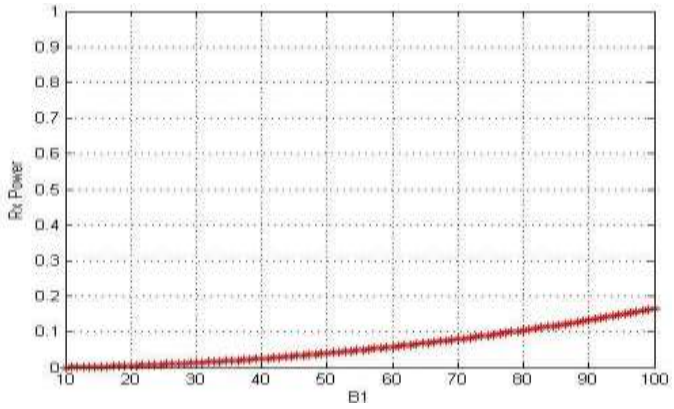

Fig 5 (b) Relation between R_x V/s Magnetic field density

V. Conclusion

Results of the discriminator experiments are generally consistent with those obtained for the respective classifiers. SVC with the radial basis kernel is the best choice for the classifier. The most successful segmentation methods are HMM and sliding window. It can be seen that the best performance is achieved by classifiers which combine features from the whole image and sub-image regions, in particular for the SVC based discriminator. Indeed, the stomach/intestine discriminator error of 100 frames constitute only four seconds of fast-forward viewing and the error of 500 frames of the intestine/colon discriminator, 20 seconds viewing time. These times are based on the clinician watching the video at 25 frames per second and would vary with viewing speed, which is usually lower. Nevertheless, we have shown that such tools can shorten the time required to annotate GI transition points, and hence significantly reduce the video viewing time.

VI References:

[1] Shi Yu, Yan Guozheng, Jia Zhiwei, Zhu Bingquan paper entitled ―The Design and Implementation of the Wireless Power Transmission System of Video Capsule Endoscopy‖ IEEE,2012 International Conference on Biomedical Engineering and Biotechnology, pp. 578-581 Chaina [2012].

[2] Carta R, Sfakiotakis M, Pateromichelakis N, Thone J, Tsakiris D P Puers R, ―A multi-coil inductive powering system for an endoscopic capsule with vibratory actuation,‖ Sensors Actuators A: Physical. Vol 172, 253-258, 2011.

[3] Carta R, Thone J Puers R, ―A wireless power supply system for robotic capsular endoscopes,‖ Sensors Actuators A162 177–83 2010.

[4] E. Scapa, H. Jacob, S. Lewkowicz, M. Migdal, D. Gat, A. Gluck-hovski, N. Gutmann, Z. Fireman, ―Initial experience of wireless-capsule endoscopy for evaluating occult gastrointestinal bleeding and suspected small bowel pathology,‖ *Amer. J. Gastro.*, vol. 97, no. 11, pp. 2776–2779, 2002.

[5] M. Mylonaki, A. Fritscher-Ravens, P. Swain, ―Wireless capsule endoscopy: A comparison with push enteroscopy in patients with gastroscopy and colonoscopy negative gastrointestinal bleeding,‖ *Gut*, vol. 52, pp. 1122–1126, 2003.

[6] R. Eliakim, ―Wireless capsule video endoscopy: Three years of experience,‖ *World J.Gastro.*, vol. 10, no. 9, pp. 1238–1239, 2004.

[7] N. Dai, C. Gubler, P. Hengstler, C. Meyenberger, P. Bauerfeind, ―Improved capsule endoscopy after bowel preparation,‖ *Gastrointest. Endoscopy*, vol. 61, no. 1, pp. 28–31, 2005.

[8] W. Selby, ―Complete small-bowel transit in patients undergoing capsule endoscopy: Determining factors and improvement with metoclopramide,‖ *Gastrointest. Endoscopy*, vol. 61, no. 1, pp. 80–85, 2005.

[9] K. H. Chong, A. C. F. Taylor, A. M. Miller, P. V. Desmond, ―Initial experience with capsule endoscopy at a major referral hospital,‖ *Med. J. Australia*, vol. 178, pp. 537–540, 2003.

[10] J. H. Lee, H. J. Park, Y. K. Moon, B. S. Song, C. H. Won, H. C. Choi, J. T. Lee, J. H. Cho, ―Design and implementation of the CPLD controller for Bi-directional wireless capsule endoscopy,‖ in *Proc. Int. Tech. Conf. Circuits/Systems, Computers and Communications*, Miyagi, Japan, Jul. 2004.

[11]D. Turgis, R. Puers, ―Image compression in video radio transmission for capsule endoscopy,‖ presented at the Eurosensors XVIII, Rome, Italy, Sep. 2004.

[12]V.S.Kodogiannis,M.Boulougoura,E.Wadge,― The usage of soft-computing methodologies in interpreting capsule endoscopy,‖ in *Comput. Biol. Med*. New York: Elsevier, 2004.